Theor Chem Acc (2011) 130:749–763
DOI 10.1007/s00214-011-0941-9

REGULAR ARTICLE

Symmetry and broken symmetry in molecular orbital description of unstable molecules IV: comparison between single- and multi-reference computational results for antiaromtic molecules

Toru Saito · Satomichi Nishihara · Shusuke Yamanaka · Yasutaka Kitagawa · Takashi Kawakami · Satoru Yamada · Hiroshi Isobe · Mitsutaka Okumura · Kizashi Yamaguchi

Received: 26 December 2010 / Accepted: 6 April 2011 / Published online: 3 June 2011

Abstract First principle calculations of the effective exchange integrals (J) in the Heisenberg model for diradical species are presented for both symmetry-adapted multi-reference (MR) and single-reference broken-symmetry (BS) methods. The Mukherjee-type state-specific MR coupled cluster singles and doubles (MkCCSD) method with several different reference orbitals including BS natural orbitals is used to calculate the singlet–triplet energy gaps (S–T energy gap or $2J$) and diradical characters for the antiaromatic molecules [**a** cyclopropenyl anion (CPA), **b** cyclobutadiene (CBD), and **c** cyclopentadienyl cation (CPC)], the cyclobutadiene derivatives with polar substitutents [**d** aminocyclobutadiene (ACBD), **e** formylcyclobutadiene (FCBD), and **f** 1-amino-2-formyl-cyclobutadiene (AFCBD)] and finally the cyclobutadine derivatives with radical substitutents [**g** 1,2-bis(methylene)cyclobutadiene (1,2-BMCBD) and **h** 1,3-bis(methylene)cyclobutadiene (1,3-BMCBD)]. For the BS methods, the spin-unrestricted Hartree–Fock based CCSD (UHF-CCSD), the CCD with the spin-unrestricted Brueckner determinant (UBD), and BS density functional theory (UDFT) computations are performed. Comparison between MkCCSD and the UHF-CCSD results indicates that spin-contamination of UHF-CCSD solutions still remains. In comparison with UHF-CCSD, the UBD results show that spin-contamination involved in BS solutions is greatly suppressed. To eliminate the spin contamination, an approximate spin-projection (AP) scheme is applied to the BS solutions. The AP procedure with the use of the expectation value of the total-spin operator corresponding to UHF-CCSD and UBD results yields good agreement with the MkCCSD results. As for the AP correction of the UDFT methods, three different computational schemes for predicting the expectation value of the total-spin operator are examined. Systematic comparisons between these methods are presented for the S–T energy gaps ($2J$). Implications of the present computational results have been discussed in relation to the design of magnetic oligomers and polymers.

Keywords Multireference coupled cluster · Diradical character · Approximate spin projection procedure · Spin contamination

Dedicated to Professor Akira Imamura on the occasion of his 77th birthday and published as part of the Imamura Festschrift Issue.

Electronic supplementary material The online version of this article (doi:10.1007/s00214-011-0941-9) contains supplementary material, which is available to authorized users.

T. Saito · S. Nishihara · S. Yamanaka · Y. Kitagawa · T. Kawakami · S. Yamada · H. Isobe · M. Okumura
Department of Chemistry, Graduate School of Science, Osaka University, 1-1 Machikaneyama, Toyonaka, Osaka 560-0043, Japan

K. Yamaguchi
NanoScience Design Center, Osaka University, 1-3 Machikaneyama, Toyonaka, Osaka 560-8531, Japan

K. Yamaguchi (✉)
TOYOTA Physical and Chemical Research Institute, Nagakute, Aichi 480-1192, Japan
e-mail: yama@chem.sci.osaka-u.ac.jp

1 Introduction

Effective exchange interactions in molecular magnetic materials have been of current interest because of their contributions to spin correlation, spin frustration, organic ferromagnetism, molecular spintronics, and so on [1–6]. Several theoretical models have indeed been applied for

first-principle calculations of these interactions to derive spin alignment rules and spin-dependent phenomena [7–10]. In past decades single-reference broken-symmetry (BS) methods have been utilized as convenient and practical procedures for estimating effective exchange integrals (J) in diradicals and polyradicals [11–14], but these methods involve spin-contamination in finite quantum systems [15–18]. The spin-contamination effect in the spin-unrestricted Hartree–Fock (UHF) and UHF based coupled cluster singles and doubles (UHF-CCSD) has also been investigated by several researchers [19–25]. We have also pointed out that the UHF-CCSD method does not completely eliminate spin-contamination, whereas the use of an approximate spin projection (AP) method greatly improved the results, reduces the remaining spin-contamination's contribution to the energy [24]. In Parts I-III of this series [26–28], we studied axial, helical, and general spin structures at the UHF, the spin-unrestricted density functional theory (UDFT), the resonating BS, and the general HF levels. These studies revealed that the BS methods with the AP correction have the potential to deal with magnetic properties of even large diradical systems. To treat polyradical and spin-frustrated systems like polynuclear transition metal complexes, further development of the usual singe reference BS, generalized HF- and/or DFT-based methods will be needed. It will be also important to consider a way of eliminating spin-contamination from these methods.

Many types of multireference (MR) methods have also been formulated and implemented since these methods are free from uncertainties related to spin-contamination [29–32]. In particular, the Mukherjee-type state-specific multireference coupled cluster singles and doubles (MkCCSD) method is intruder-free and satisfies the size-extensive condition, which is essential for large systems [31, 33–35]. Very recently, Evangelista et al. [34] demonstrated that it is crucial to use the MkCCSD method in combination with the localized active orbitals obtained from a complete active space self-consistent field (CASSCF) calculation to obtain the size-consistent correction. Unfortunately, the present applicability of the MkCCSD method is limited to small diradical systems. For larger systems and polyradical systems such as transition metal complexes, the difference dedicated configuration interaction (DDCI) method and the second-order perturbation theory based on the CASSCF wave function such as CASPT2 and NEVPT2 are more practical within a framework of ab initio wave function theories [36–39]. The density matrix renormalization group (DMRG) methods are also under development to describe nondynamical correlation effects in large active spaces [40]. As a competitive alternative to MR wave function theories, the MR version of DFT (CAS-DFT) method has also been developed by our group and other groups [41–47]. If several difficulties, including the double-counting problem, can be overcome, then it will be possible that CAS-DFT will be able to describe both the nondynamical and dynamical correlation effects in a balanced way at lower computational costs than the current CASPT2 method [46]. On the other hand, Weimer et al. [48] proposed the multiconfiguration optimized effective potential (MCOEP) method to treat nondynamical correlation effects within a DFT framework. Despite low computational costs of DFT methods, practical pure and hybrid DFT methods are less reliable than ab inito wave function based methods. With Barlett groups ab intio DFT methods, one now needs to distinguish ab inito WFT and ab initio DFT, as they are different. The KS-DFT method uses the non-interacting electron kinetic energy functional, Ts, which has a corrections T-Ts, in addition to the electron exchange and electron correlation functionals, which need to be determined more accurately and systematically to achieve chemical accuracy for all of the elements in the periodic table [49].

Quasi-degenerate systems are currently being investigated using both BS and MR methods. As a first step in the design of molecular-based magnetic materials, we employ both the MR methods and BS methods for the understanding of small systems with complicated electronic structures. Since the highly accurate MkCCSD method yields reliable benchmark results for small diradical species [34, 50, 51], we will show by comparison with the MkCCSD results that the AP method by eliminating spin-contamination effects improves UHF-CCSD results (energies). In addition to UHF-CCSD, the CCD method using the spin-restricted Brueckner determinant (UBD) [52, 53] is also examined to compare the performance between the use of the UHF determinant with the use of the Brueckner determinant. We also apply the AP scheme to the UDFT solutions. For the estimation of $\langle S^2 \rangle$ values, in addition to the conventional non-interacting procedure [54], the exchange local spin density (XLSD) scheme [55] and the exchange generalized gradient approximation (XGGA) scheme [56] are employed. The diradical systems considered in this study are as follows: the antiaromatic molecules [**a** cyclopropenyl anion (CPA), **b** cyclobutadiene (CBD), and **c** cyclopentadienyl cation (CPC)], the cyclobutadiene derivatives with polar substitutents [**d** aminocyclobutadiene (ACBD), **e** formylcyclobutadiene (FCBD), and **f** 1-amino-2-formyl-cyclobutadiene (AFCBD)} and finally the cyclobutadine derivatives with radical substitutents [**g** 1,2-bis(methylene)cyclobutadiene (1,2-BMCBD) and **h** 1,3-bis(methylene)cyclobutadiene (1,3-BMCBD)]. The systematic comparisions of the S–T energy gaps ($2J$) of these diradical species calculated with several BS methods with those obtained with the MkCCSD methods are used to elucidate their scope and applicability for

treating (to calculate the energies for these) exchange coupled systems.

2 Theoretical background and computational methods

2.1 Natural orbitals, localized natural orbitals and their classifications

The instability problem for closed-shell methods requires one to derive the expressions for the corresponding BS methods [57, 58]. To investigate and elucidate the static electron and spin correlation effects involved in the BS methods, the first-order density matrix $\rho(\mathbf{r},\mathbf{r}')$ obtained for these BS methods is diagonalized [15, 23] as

$$\rho(\mathbf{r},\mathbf{r}') = \sum_i n_i \phi_i^*(\mathbf{r})\phi_i(\mathbf{r}'), \tag{1}$$

where ϕ_i and n_i are, respectively, the natural orbitals (NOs) and the occupation numbers of the BS solutions. The BS molecular orbitals (MOs) of these solutions are expressed with the symmetry-adapted bonding (ϕ^b) and antibonding (ϕ^a) MO pair as

$$\psi_i^{\pm} = \cos\theta_i \phi_{\mathrm{MO}}^b \pm \sin\theta_i \phi_{\mathrm{MO}}^a, \tag{2}$$

where θ denotes the orbital mixing parameter determined by BS computations [59–61]. BS MOs are often spatially symmetry-broken because ϕ_{MO}^b and ϕ_{MO}^a are symmetry-adapted and usually belong to different spatial symmetries [23, 62].

The active NOs with occupation numbers close to 1.0 are responsible for the nondynamical correlation effects in this scheme [24, 63]. On the other hand, the core and virtual NOs are utilized for inclusion of dynamical correlation effects. Several chemical indices are introduced to elucidate the nature of chemical bonds in diradical species [24]. The orbital overlap S_i between BS MOs under the corresponding orbital transformation [61, 64] is defined as

$$S_i = \langle \psi_i^+ | \psi_i^- \rangle = \cos 2\theta_i. \tag{3}$$

Then S_i becomes 1.0 for the closed-shell (restricted) systems, whereas S_i is 0.0 ($\theta = \pi/4$) for the complete diradical species [64]. To express a quantitative description of chemical bonding under the BS approximation, the effective bond order b_i is defined as

$$b_i = \frac{n_i - n_i^*}{2} = S_i, \tag{4}$$

where n_i and n_i^* denote the occupation numbers of the bonding and antibonding NOs, respectively [24]. Therefore, the effective bond order (b_i) is equal to S_i. The localized NOs are therefore defined as the completely spin polarized BS MOs as [24, 50]

$$\psi^{\pm}(\theta = \pi/4) = \frac{1}{\sqrt{2}}\left(\phi_{\mathrm{NO}}^b \pm \phi_{\mathrm{NO}}^a\right). \tag{5}$$

It is important to use localized UHF NOs (UNOs), CASSCF NOs, and UDFT Kohn-Sham NOs (DNOs) as well as ROHF MOs for MkCCSD computations to be size-consistent.

The biorthogonalization of the canonical BS MOs provides the corresponding molecular orbitals (CMOs) [24, 62], such that the α and β BS MOs have the maximum overlap.

$$\psi^{\pm}(\mathrm{CMO}) = \cos\theta \phi_{\mathrm{NO}}^b \pm \sin\theta \phi_{\mathrm{NO}}^a, \tag{6a}$$

where ϕ_{NO}^b and ϕ_{NO}^b represents the bonding and antibonding NO pair. The total spin quantum number $\langle \mathrm{S}^2 \rangle$ value of singlet open-shell species by the BS calculations are directly related to the maximum orbital overlaps between CMOs

$$\langle S^2 \rangle = \sum_{i=1}^{m} \left(1 - S_i^2\right). \tag{6b}$$

The diradical character defined with the weight of doubly excited configuration in the CI method is also expressed with the orbital overlap under the spin-projected BS solutions as [24]

$$Y_i = 2W_{\mathrm{D}} = \frac{(1-S_i)^2}{1+S_i^2} = 1 - \frac{2S_i}{1+S_i^2}. \tag{6c}$$

The diradical character is directly related to the effective bond order after the spin projection as

$$B_i = 1 - Y_i = \frac{2S_i}{1+S_i^2}. \tag{6d}$$

2.2 Computational schemes of effective exchange integrals

Appropriate modeling of quantum mechanical computational results is crucial for the analysis and modeling of molecule-based magnetic materials. The effective exchange interactions for diradical species have been described by the Heisenberg spin Hamiltonian as [1–16]

$$H_{\mathrm{Heisenberg}} = -2J\mathbf{S}_1 \cdot \mathbf{S}_2, \tag{7}$$

where $\mathbf{S}_1$ and $\mathbf{S}_2$ are spin operators for each site and J is an effective exchange integral. After the AP correction, the J value can be derived as [13]

$$J_1 = \frac{E^{\mathrm{LS}} - E^{\mathrm{HS}}}{\langle \mathbf{S}^2 \rangle^{\mathrm{HS}} - \langle \mathbf{S}^2 \rangle^{\mathrm{LS}}}, \tag{8a}$$

where LS and HS denote, respectively, the total lowest spin and highest spin states of the exchange-coupled systems; E and $\langle \mathrm{S}^2 \rangle$ denote the total energy and total spin angular

momentum, respectively. The $\langle S^2 \rangle^{LS}$ value obtained by BS methods are not always zero even for singlet diradicals, indicating that $\langle S^2 \rangle^{LS}$ is a measure of spin contamination in the BS solutions as shown in Eqs. 6a, 8a can be applicable to symmetry-adapted RHF-CC and MkCCSD methods [13, 24, 51, 65]. It can be reduced to the weak [14] and strong [11, 12] correlation limits as follows:

$$J_2 = \frac{E^{\mathrm{LS}} - E^{\mathrm{HS}}}{S_{\max}(S_{\max}+1)}, \tag{8b}$$

$$J_3 = \frac{E^{\mathrm{LS}} - E^{\mathrm{HS}}}{S_{\max}^2}, \tag{8c}$$

where $S_{\max}$ denotes the spin quantum number of the total highest spin state of an exchange-coupled system; Eqs. 8b and 8c have been utilized for BS solutions.

Our AP scheme removes approximately the spin-contamination effect from the UHF based methods and UDFT [24]. In fact, the AP method has performed well for magnetic clusters and polymers [66–69]. The extrapolation with Eq. 8a yields the total energy of the pure LS state approximately as [24]

$$E^{\mathrm{AP}} = E^{\mathrm{LS}} - J_1\left(S_z^{\mathrm{LS}}(S_z^{\mathrm{LS}}+1) - \langle \mathbf{S}^2 \rangle^{\mathrm{LS}}\right) \tag{9}$$

The AP scheme is utilized for simple quantum spin correction for BS energy. The S–T gaps (2 J) are regarded as the resonance energy that is used to confirm the scope and applicability of various computational methods because it can be determined experimentally [66–69].

2.3 Spin contamination error and $\langle S^2 \rangle$ of several BS solutions

To investigate the spin-contamination effect of the BS methods, an appropriate evaluation of the $\langle S^2 \rangle$ value is required. Although $\langle S^2 \rangle$ values of UHF solutions can be calculated easily and uniquely as shown in Eq. 6a, it is difficult to calculate $\langle S^2 \rangle$ values of UHF-CC solutions because CC methods are not variational and require huge computational costs. In this study, we adopt the scheme proposed by Purvis et al. [54],

$$\langle \mathbf{S}^2 \rangle_{\mathrm{UHF-CC}} \approx \frac{\langle \Psi_{\mathrm{UHF}} | \mathbf{S}^2 | \Psi_{\mathrm{UHF-CC}} \rangle}{\langle \Psi_{\mathrm{UHF}} | \Psi_{\mathrm{UHF-CC}} \rangle}, \tag{10}$$

which takes lower computational costs. While more accurate formalisms of $\langle \mathbf{S}^2 \rangle_{\mathrm{UHF-CC}}$ have been proposed [20, 21], Eq. 10 provides a good approximation.

The UDFT calculations are useful for large radical systems [66–75]. The UDFT methods have been successfully applied to the prediction of activation barriers of chemical reactions, magnetic properties, and so on. However, the spin-contamination is a serious problem for UDFT solutions because there is no explicit formalism to compute their $\langle S^2 \rangle$ values. Recently, the non-interacting Kohn–Sham single determinant wave functions have been usually assumed to compute $\langle S^2 \rangle$ values. In addition to the standard non-interacting procedure [54], the exchange spin density (XLSD) scheme proposed by Wang et al. [55] is used.

$$\langle \mathbf{S}^2 \rangle_{\mathrm{XLSD}} = S_z(S_z+1) - \int_{\rho_s(\mathbf{r})<0} \rho_s(\mathbf{r}) \mathrm{d}\mathbf{r}, \tag{11}$$

where $\rho_s(\mathbf{r})$ is the spin-density and S_z is the z-component of the total spin. The XLSD scheme is based on the Löwdin's expression [17] for the $\langle S^2 \rangle$ based on two-electron density matrix, and reducing to one-electron density matrix with an assumption of the Slater-determinant-like notation. The exchange generalized gradient approximation (XGGA) scheme including Becke88 exchange functional [76] proposed by Cohen et al. [56] is also employed.

$$\langle \mathbf{S}^2 \rangle_{\mathrm{XGGA}} = S_z(S_z+1) + N_\beta - \int \rho_\sigma(\mathbf{r})\, d\mathbf{r}, \begin{cases} \sigma = \alpha & \text{if } k_\alpha^{\mathrm{XGGA}}(\mathbf{r}) \le k_\beta^{\mathrm{XGGA}}(\mathbf{r}) \\ \sigma = \beta & \text{if } k_\alpha^{\mathrm{XGGA}}(\mathbf{r}) > k_\beta^{\mathrm{XGGA}}(\mathbf{r}) \end{cases} \tag{12}$$

where N_β is the number of β-electrons and $k_\sigma^{\mathrm{XGGA}}(\mathbf{r})$ is defined as

$$k_\sigma^{\mathrm{XGGA}}(\mathbf{r}) = \left[\frac{9\pi}{K_\sigma^{\mathrm{XGGA}}(\mathbf{r})}\right]^{1/2} \rho_\sigma^{1/3}(\mathbf{r}),$$
$$E_{\mathrm{Becke88}} = -\frac{1}{2}\sum_\sigma \int \rho_\sigma^{4/3}(\mathbf{r})\, K_\sigma^{\mathrm{XGGA}}(\mathbf{r}) \mathrm{d}\mathbf{r}. \tag{13}$$

2.4 Spin projection for UHF-CCSD

The AP procedure is examined in relation to the MkCCSD method (its detail is given in the supporting material). In UHF-CCSD calculation based on the UHF ($S_z = 0$) reference function, projected energy E_{prj1}, in which triplet contamination is annihilated, is formally identical to non-projected energy $E_{\mathrm{UHF-CCSD}}$ as

$$E_{\mathrm{prj1}} \equiv \frac{\langle \Phi | A_1 H e^{T_1+T_2} | \Phi \rangle}{\langle \Phi | A_1 e^{T_1+T_2} | \Phi \rangle} \tag{14}$$

$$= \frac{\sum_p^{0,S,D} \langle \Phi | A_1 | \Phi_p \rangle \langle \Phi_p | H e^{T_1+T_2} | \Phi \rangle}{\langle \Phi | A_1 e^{T_1+T_2} | \Phi \rangle} \tag{15}$$

$$= \frac{E_{\mathrm{UHF-CCSD}} \sum_p^{0,S,D} \langle \Phi | A_1 | \Phi_p \rangle \langle \Phi_p | e^{T_1+T_2} | \Phi \rangle}{\langle \Phi | A_1 e^{T_1+T_2} | \Phi \rangle} \tag{16}$$

$$= E_{\mathrm{UHF-CCSD}}, \tag{17}$$

where $A_1 = \mathbf{S}^2 - 2$ is a projection operator and $|\Phi\rangle$ is a UHF wave function [17]. In Eqs. 15 and 16, summations in

numerator run over ground state (0), single excited states (S) and double excited states (D). Also in Eq. 16, we have used the definition of the CCSD energy

$$\langle\Phi|He^{T_1+T_2}|\Phi\rangle = E_{\mathrm{UHF-CCSD}}, \tag{18}$$

and the amplitude equations

$$\begin{aligned}\left\langle\Phi_i^a|He^{T_1+T_2}|\Phi\right\rangle &= E_{\mathrm{UHF-CCSD}}\left\langle\Phi_i^a|e^{T_1+T_2}|\Phi\right\rangle \\ \left\langle\Phi_{ij}^{ab}|He^{T_1+T_2}|\Phi\right\rangle &= E_{\mathrm{UHF-CCSD}}\left\langle\Phi_{ij}^{ab}|e^{T_1+T_2}|\Phi\right\rangle.\end{aligned} \tag{19}$$

Annihilating the singlet state yields projected energy E_{prj2}, which is identical to the non-projected UHF-CCSD energy as

$$E_{\mathrm{prj2}} = \frac{\langle\Phi|A_2\,He^{T_1+T_2}|\Phi\rangle}{\langle\Phi|A_2\,e^{T_1+T_2}|\Phi\rangle} = E_{\mathrm{UHF-CCSD}}, \tag{20}$$

where $A_2 = \mathbf{S}^2$ annihilates the contribution from the singlet state. E_{prj1} and E_{prj2} are total energies corresponding to the LS and HS states, respectively. However, Eqs. 17 and 20 lead to a wrong conclusion that the HS and LS states are always degenerate in energy. This HS–LS degeneracy contradicts previous results [24], and suggests the failure of the spin-projection scheme defined in Eq. 14. In fact, we revealed that the potential energy curve of F_2 molecule obtained by UHF-CCSD was quite different from that obtained by MkCCSD, whereas the UHF-CCSD with the AP correction well reproduced the MkCCSD calculation [51]. It is caused by neglecting relaxation of CCSD amplitudes ($T1 + T2$) during the scheme. In other words, the projected amplitude equation should be solved to obtain projected LS energy (E_{prj1}) and wave function.

$$\begin{aligned}\left\langle\Phi_i^a|A_1\,He^{T_1+T_2}|\Phi\right\rangle &= E_{\mathrm{prj1}}\left\langle\Phi_i^a|A_1\,e^{T_1+T_2}|\Phi\right\rangle \\ \left\langle\Phi_{ij}^{ab}|A_1\,He^{T_1+T_2}|\Phi\right\rangle &= E_{\mathrm{prj1}}\left\langle\Phi_{ij}^{ab}|A_1\,e^{T_1+T_2}|\Phi\right\rangle\end{aligned} \tag{21}$$

Note that the spin-projected energy and amplitude equations should be defined in Eqs. 14 and 21, respectively, if the projected CCSD wave function is assumed as $A_1\,e^{T_1+T_2}|\Phi\rangle$. On the other hand, in Ref. [22], only the energy was projected by Eq. 14 and determined by the non-projected amplitude equation (Eq. 21). The discrepancy between the projected energy and non-projected amplitudes causes an incorrect behavior ($E_{\mathrm{UHF-CCSD}} = E_{\mathrm{prj1}} = E_{\mathrm{prj2}}$). In other words, if the post-HF wave function is assumed as $\sum_i C_i|i\rangle$, both Slater determinants $\{|i\rangle\}$ and expansion coefficients $\{C_i\}$ should be projected, whereas the projection was considered only for $\{|i\rangle\}$ in Ref. [22].

The projected amplitude equation (Eq. 21) appears in the MkCCSD computations (see supporting material). The amplitude of MkCCSD is adapted not to the single-reference CC wave function, but to MkCCSD one. On the other hand, UHF-CCSD with the AP correction partly involves the relaxations of MOs and amplitude, leading to approximately good results. In this work, we use the AP method instead of the above spin-projection scheme (Eqs. 14 and 21) due to its ease of use and low computational costs in addition to the size-consistency.

2.5 Computational details

Figure 1 illustrates the computational schemes of the effective exchange integrals starting from the BS computations towards the MkCCSD computations as mentioned in Sect. 2.1. The localization of the active orbitals is performed by using Eq. 5. Our basic ideas [24] are selections of the minimal active space on the basis of the occupation numbers of the NOs obtained by BS solutions. Therefore, the minimal active space (2,2) (2 electrons in 2 orbitals) incorporates only static electron correlation. The remaining dynamical correlation effects are included by the CC techniques instead of the CASPT2 methods. If we employ the CASPT2 procedures, active spaces are taken to be large (or full valence) to obtain reasonable computational results. On the other hand, appropriate selections of excitation operators such as SDT… are required in the CC approach. In this paper, we have performed both the BS and MkCCSD computations of typical diradical species: antiaromatic molecules (**a**–**c**), cyclobutadiene derivatives with polar substituents (**d**–**f**) and cyclobutadiene with radical substituents (**g**–**h**) as shown in Fig. 2. The J values are obtained using Eqs. 8a, b, c. Full geometry optimizations were performed by UHF-CCSD for **a**-**c** and UCAM-B3LYP for **d**–**j**. The geometries of both the BS singlet the triplet states were optimized for **g** and **h**, respectively, while the geometries for the triplet states were optimized for the others. The optimized geometries are given in the supporting materials.

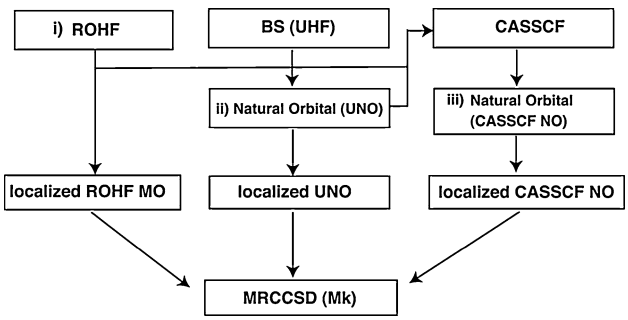

Fig. 1 Computational schemes for electronic and spin states of quasi-degenerate systems such as antiaromatic molecules by using the MkCCSD and related methods. The minimal active space used to incorporate non-dynamical correlation effects. The dynamical correlation effects are calculated by the CC methods

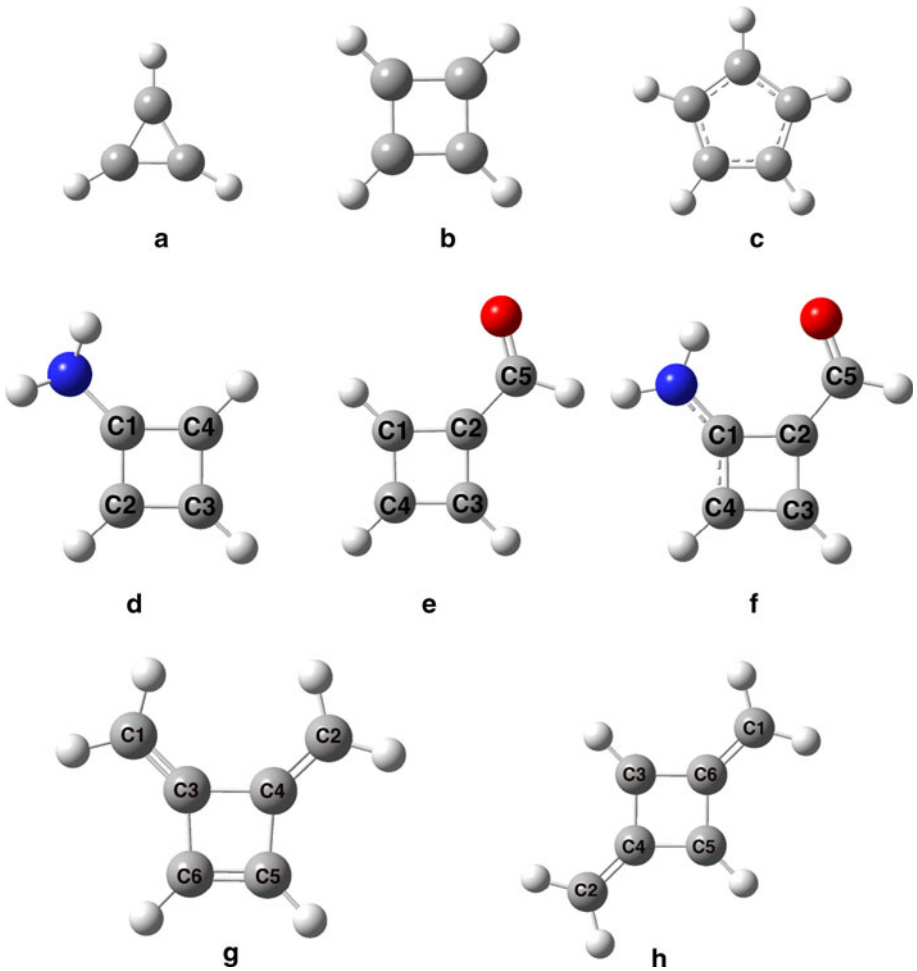

Fig. 2 Molecular structures of antiaromatic molecules (**a**–**c**), cyclobutadienes with polar substituents (**d**–**f**) and bis(methylene)cyclobutadiene isomers (**g**, **h**)

The HF, post-HFs and DFT calculations have been performed by Gaussian program package [77]. The CASSCF calculations have been performed by GAMESS program package [78, 79] and MkCCSD calculations have been performed by PSI3 program package [80]. For all calculations, we have employed the aug-cc-pVDZ basis set for **a** and cc-pVDZ for the others [81, 82]. Spin-unrestricted type of BLYP, B3LYP, BHandHLYP, LC-BLYP and CAM-B3LYP were employed in DFT computations [83–86].

3 Computational results for parent antiaromatic molecules

3.1 HF instability and symmetry breaking in antiaromatic molecules

As shown in Fig. 2, three antiaromatic molecules; cyclopropenyl anion $C_3H_3^-$ (**a**), cyclobutadiene C_4H_4 (**b**), and cyclopentadienyl cation $C_5H_5^+$ (**c**) have been investigated by both in the experimental and theoretical methods [87–101]. Hund's rule [1] predicts the ground triplet state of cyclobutadiene (**b**) at the square planar conformation without the Jahn–Teller distortion (lattice symmetry breaking or bond alternation) because of the complete HOMO-LUMO degeneracy. This is, however, a typical example of the breakdown of Hund's rule [1, 8, 9]. In fact, early theoretical studies such as CI, UHF and resonating generalized valence-bond (RGVB) methods had already revealed that the dynamic spin-polarization (SP) effect yields the singlet ground state even at the D_{4h} conformation [8, 88–94]. Recent more rigorous theoretical computations supported previous predictions [96, 99]. The ESR spectroscopy [89] has demonstrated that cyclopentadienyl cation has the triplet ground state with the D_{5h} conformation; this conformation is aromatic in the triplet state [87].

The RHF solutions for **a**–**c** suffer from the triplet instability (or spin instability) [8, 59, 90] because of the HOMO-LUMO degeneracy [87]. This entails the reorganization of the RHF solutions into the more stable singlet UHF solutions via HOMO-LUMO mixing [8] (see Eq. 2) that induces inevitably the orbital and spin-symmetry breaking [8, 9, 90, 91]. The spin-symmetry breaking brings about the non-zero $\langle S^2 \rangle^{LS}$ values even for singlet diradicals as shown in Table 1.

Table 1 Total spin angular momentums $\langle S^2 \rangle$ (The non-interaction method is used) of antiaromatic molecules by the BS methods

Method	$C_3H_3^-$ (**a**)		C_4H_4 (**b**)		$C_5H_5^+$ (**c**)	
	LS	HS	LS	HS	LS	HS
UHF	1.0508	2.0216	1.2498	2.0148	1.1731	2.0119
UHF-MP2	1.0670	2.0042	1.1630	2.0010	1.1443	2.0001
UHF-CCSD	1.0735	2.0014	0.9856	2.0010	1.0692	2.0009
UBLYP	1.0067	2.0034	1.0314	2.0032	1.0149	2.0026
UB3LYP	1.0107	2.0050	1.0559	2.0044	1.0304	2.0035
UCAM-B3LYP	1.0126	2.0093	1.0745	2.0047	1.0455	2.0039
UBHandHLYP	1.0196	2.0093	1.1049	2.0070	1.0641	2.0056
ULC-BLYP	1.0149	2.0076	1.1010	2.0053	1.0691	2.0045
UBD	1.0819	2.0008	0.9683	2.0007	1.0678	2.0006

The $\langle S^2 \rangle^{LS}$ value theoretically becomes almost 1.0 in the case of the complete mixing of the π-type HOMO and LUMO; namely (π, π) singlet diradical state of **a**. However, it becomes larger than 1.0 for **b** and **c** as shown in Table 1. It implies that the spin polarization (SP) of other π-electrons is non-negligible [8, 9, 90, 91]. The π-(HOMO-1) and π-(LUMO +1) mixing in Eq. 2 occurs via the intramolecular magnetic fields of the π-diradical electrons [1, 24]; the negative spin densities appears on the carbon atoms via this SP effect. Therefore, the SP effect cased by the UHF approximation is often expressed with the use of the spin vector model as illustrated in Fig. 3 [24, 63]. The up- and down-arrows mean the α and β spin densities, respectively. The spin densities on the carbon atoms of **a**–**c** obtained by the LS and HS solutions are summarized in the Tables S2–S4 in the Supporting Information. Judging from the $\langle S^2 \rangle^{HS}$ values and positive spin densities on all carbon atoms for **a**–**c** as listed Tables S2–S4 in the Supporting Information, the SP effect of π-electrons is not significant in the triplet state. The antiferromagnetic alignment of spin densities for **b** and **c** by UHF is in accord with the spin vector model A (B) and C in Fig. 3. However, the magnitude of the spin densities is too large because of the too much SP effect of π-electrons under the UHF approximation. This tendency is not remarkable for **a**.

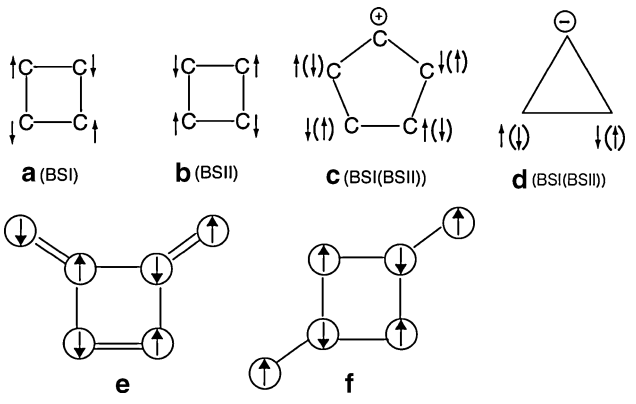

Fig. 3 Spin vector models for spin alignments via the spin polarization or spin delocalization effects for antiaromatic molecues (**a**–**c**) and bis(methylene)cyclobutadiene isomers (**g**, **h**)

The dynamical correlation corrections for the UHF solutions are examined by using the UHF-MP2 and UHF-CCSD methods as shown in Table 1. The reduction of the $\langle S^2 \rangle^{LS}$ values by UHF-MP2 is rather small (0.04–0.08) for **b** and **c**, indicating that the spin contamination effects via the SP effect still remain [24]. On the other hand, the $\langle S^2 \rangle^{LS}$ values obtained by the UHF-CCSD method almost 1.0 for these species, indicating the significant elimination of the spin contamination via the (HOMO − 1)–(LUMO + 1) mixing. However, the spin contamination effects are not completely eliminated at the CCSD level, in contrast to the previous theoretical predictions [22]. Moreover the $\langle S^2 \rangle^{LS}$ values of **a** increase with the correlation corrections. This means that the UHF-CC methods including much higher excitation operators like UHF-CCSDTQ [25] are desirable for the further improvement of the $\langle S^2 \rangle^{LS}$ values for **a**–**c**. The $\langle S^2 \rangle^{HS}$ value for **a**–**c** by UHF-CCSD is almost 2.0, showing the spin contamination errors are negligible for the triplet diradicals (**a**–**c**). The $\langle S^2 \rangle^{LS}$ values calculated by the UBD method are close to the corresponding values for **a**–**c** by UHF-CCSD. The spin densities on the carbon atoms by UBD indicate the antiferromagnetic alignment in accord with the spin vector model in Fig. 3a–c, but their magnitude is largely reduced and is consistent with the weak SP effect as shown in Tables S2–S4. The $\langle S^2 \rangle^{HS}$ value for **a**–**c** by UBD is also almost 2.0, indicating no significant SP effect. Thus the UBD method provides reasonable $\langle S^2 \rangle$ values for both the singlet and triplet states of **a**–**c**.

Figure 4 shows the π- and next π-CMOs for **b** obtained by the singlet UHF (A) and spin-unrestricted Brueckner determinant (B). Both the π-CMOs are indeed localized on the 1(2) and 3(4) carbon atoms, respectively. As for (A), the orbital overlap between next π-CMOs in Eq. 6a is smaller than 1.0, indicating that the dynamic SP effect is not negligible. Therefore, the $\langle S^2 \rangle^{LS}$ value is larger than 1.0 as listed in Table 1. On the other hand, the orbital overlap between the next π-CMOs obtained by (B) is larger than that obtained by (A). The difference is attributed to the fact that the π-type SP effects are largely suppressed in (B). The orbital overlaps for **a**–**c** calculated at UDFT levels are shown in Tables S5–S7.

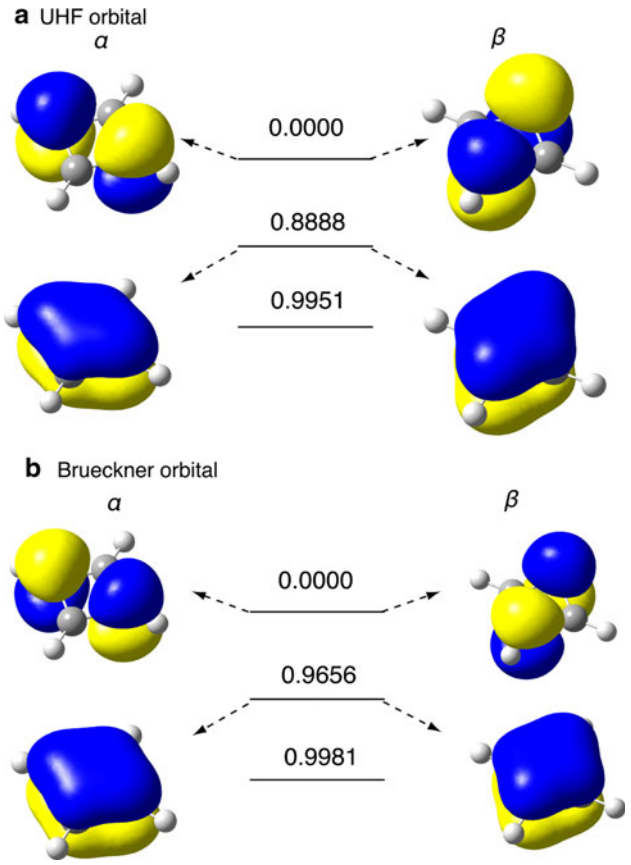

Fig. 4 Corresponding molecular orbitals (CMO) from UHF (**a**) and spin-unrestricted Brueckner (**b**) orbitals for **b** with orbital overlap (S_i) values

3.2 Post-UHF and UBD calculations of 2*J* values in antiaromatic molecules

Table 2 summarizes the 2*J* values for **a**–**c** obtained by three procedures in Eqs. 8a, b, c based on the R(U)HF and related correlation methods. First of all, let us examine the RHF-based computations of *J* values for antiaromatic molecules for the comparative purposes. Table 2 summarizes the S–T gaps (2 *J*) for **a**–**c** by R(O)HF methods. Judging from the large positive 2*J* values, the RHF solution cannot properly describe the singlet (π, π) diradical state. The HOMO-LUMO degeneracy of the RHF solution for **a**–**c** also entails the breakdown of post-RHF methods and this tendency is not improved at the RHF-CCSD and RHF-CCSD(T) levels. The RHF-based the equation-of-motion CCSD (EOM-CCSD) together with the cc-pVTZ basis sets also provided the positive 2*J* value of 13 kcal/mol, while the spin-flip EOM-CCSD method reproduced the singlet ground state [96]. From Table 2, the 2*J* value for **a** is positive at the UHF level, but the results are negative for **b** and **c** because of the strong SP effect in the singlet state as illustrated in Fig. 3. On the other hand, the 2*J* values at the

Table 2 The 2*J* [$J = J_1$ by Eq. 8a and J_3 by Eq. 8c in the parentheses ($J_3 = 2J_2$ by Eq. 8b)] values (kcal/mol) for antiaromatic molecules calculated by the BS and MR methods

Method	$C_3H_3^-$ (**a**)	C_4H_4 (**b**)	$C_5H_5^+$ (**c**)
UHF	20.9 (20.3)	−62.2 (−47.6)	−9.2 (−7.8)
R(O)HF	49.7	33.1	34.0
R(O)MP2	760	14.2	26.5
R(O)CCSD	72.8	10.5	22.9
R(O)CCSD(T)	73.0	4.0	20.3
UHF-MP2	19.3 (18.1)	14.8 (12.4)	39.2 (33.5)
UHF-CCSD	15.5 (14.4)	−9.9 (−10.1)	11.1 (10.4)
UHF-CCSD(T)	12.7 (11.8)	−4.8 (−4.8)	14.8 (13.7)
UBD	15.9 (14.6)	−9.1 (−9.1)	11.8 (11.0)
UBD(T)	12.5 (11.4)	−5.1 (−5.2)	14.0 (13.0)
ROHF-MkCCSD	12.0	−8.6	13.5
CASSCF-MkCCSD	13.0	−8.1	9.4
UNO-MkCCSD	12.3	−8.9	13.8
DNO-MkCCSD	12.3	−9.0	13.7

UHF-MP2 level are positive for **a**–**c**, indicating the triplet ground state even for **b**. The UHF-CCSD method similarly predicts the triplet ground state for **a** and **c**, but it provides the negative 2*J* value for **b**. This tendency by UHF-CCSD is the same as the UHF-CCSD(T) approximation. Therefore, the UHF-CCSD and UHF-CCSD(T) methods correctly describe the dynamic SP effect for **b**. Interestingly, the 2*J* value obtained by CASSCF(2,2) is positive even for **b** because of no inclusion of this effect as shown in Table 2. The UBD calculations significantly decrease the spin-contamination effects of the UHF solutions and yield qualitatively correct values of 2*J* in combination with the AP scheme. The UHF-CCSD and UBD results are close to the spin-flip EOM-CCSD result (−8.5 kcal/mol), whereas the UHF-CCSD(T) and UBD(T) results are comparable to the MR averaged quadratic coupled cluster (MR-AQCC) result (−5.5 kcal/mol). The J_1 values by Eq. 8a [13] are close to the corresponding J_3 values by Eq. 8c [12] in the case of antiaromatic molecules with 100% diradical character. On the other hand, the J_2 value by Eq. 8b [14] is simply twice of the J_3 value in the case of diradical species with $S_{\max} = 1$. The same tendency is also observed for UDFT computations as shown below. Thus the numerical values in Tables 2 and 3 clarify the scope and applicability of the computational schemes for 2*J* values.

3.3 Spin-polarized DFT calculations of 2*J* values in antiaromatic molecules

We have used several exchange–correlation functional sets to calculate the S-T gaps (2 *J*) for antiaromatic molecules together with three different formulae in Eqs. (8a, 8b, 8c).

Table 3 The $2J$ [$J = J_1$ by Eq. 8a and J_3 by Eq. 8c in the parentheses ($J_3 = 2J_2$ by Eq. 8b)] values (kcal/mol) for antiaromatic molecules (**a**)–(**c**) by the hybrid DFT methods

Method[a]	$C_3H_3^-$ (**a**)	C_4H_4 (**b**)	$C_5H_5^+$ (**c**)
UBLYP (NI)	8.6 (8.5)	−4.2 (−4.1)	9.3 (9.2)
UBLYP (XLSD)	6.7	−4.5	7.6
UBLYP (XGGA)	6.7	−4.5	7.6
UB3LYP (NI)	11.6 (11.6)	−8.6 (−8.2)	9.1 (8.9)
UB3LYP (XLSD)	9.2	−9.8	7.8
UB3LYP (XGGA)	9.2	−9.8	7.8
UCAM-B3LYP (NI)	14.2 (14.2)	−12.9 (−12.0)	6.5 (6.2)
UCAM-B3LYP (XLSD)	11.4	−15.1	5.6
UCAM-B3LYP (XGGA)	11.4	−15.1	5.6
UBHandHLYP (NI)	15.7 (15.6)	−19.7 (−17.7)	6.3 (6.0)
UBHandHLYP (XLSD)	12.8	−24.2	5.7
UBHandHLYP (XGGA)	12.8	−24.2	5.7
ULC-BLYP (NI)	17.7 (17.5)	−20.1 (−18.2)	1.6 (1.5)
ULC-BLYP (XLSD)	14.4	−24.3	1.5
ULC-BLYP (XGGA)	14.4	−24.3	1.5

[a] NI represents the non-interacting scheme

Three different computational schemes [54–56] of the $\langle S^2 \rangle$ values by UDFT are also examined. The values of $2J$ calculated by UDFT are listed in Table 3. All the UDFT methods employed here predict the positive $2J$ values for **a** and **c**, and negative $2J$ values for **b**. The $2J$ value for **a** by UB3LYP is compatible with those of UHF-CCSD(T) and UBD(T). On the other hand, the UBD(T) value for **b** is rather close to that of UBLYP. The magnitude of $2J$ values for **a** and **b** increase in the order: UBLYP < UB3LYP < UCAM-B3LYP < UBHandHLYP < ULC-BLYP. It in turn decreases in the same order in the case of **c**. These trends are consistent with the increase of the HF exchange term. The $2J$ values for **c** by all the hybrid UDFT methods examined here are smaller than those of UHF-CCSD(T) and UBD(T).

The $2J$ values for **a** and **c** obtained by the non-interacting approximation is always larger than those obtained by the XLSD and XGGA scheme. Nevertheless, the differences in the $2J$ values between non-interacting approximation and the XLSD (or XGGA) scheme are not so large for **a**–**c** for all UDFT methods examined here. Therefore, Eq. 8a with the use of the $\langle S^2 \rangle$ values obtained by the non-interacting procedure is practical for calculating $2J$ values. Thus hybrid UDFT methods qualitatively reproduce the S–T gaps ($2J$) for antiaromatic molecules calculated by the post-UHF methods. This is the reason why previous hybrid UDFT computations have provided reasonable $2J$ values for magnetic oligomers and polymers as compared with their corresponding experimental values [66–69].

3.4 MkCCSD calculations of antiaromatic molecules

Several reference orbitals discussed in Sect. 2.5 are examined for MkCCSD computations of parent antiaromatic molecules (**a**–**c**). The NOs obtained by UCAM-B3LYP are used as DNO. As listed in Table 2, the MkCCSD calculations provide ferromagnetic coupling for **a** and **c** and antiferromagnetic coupling for **b** in accordance with the UHF-CCSD methods. The sign and magnitude of $2J$ values for **a** and **b** do not significantly vary with the reference orbitals. On the other hand, the absolute $2J$ value for **c** calculated by MkCCSD starting from CASSCF NOs is smaller than the other reference orbitals (ROHF, UNO, and DNO) by 4 kcal/mol. Since the MkCCSD method provides the negative S–T gaps ($2J$) for **b** regardless of the reference orbitals, the dynamical SP effect is correctly described by the combination of the exponential ansatz and minimal active space. The absolute $2J$ value for **b** calculated by the MkCCSD methods are close to those of UB3LYP, UBD, UHF-CCSD, and spin-flip EOM-CCSD [96], while the value is larger than those of UHF-CCSD(T) and UBD(T) by 4–5 kcal/mol. In this sense, the MkCCSD method is useful as an indicator to check the reliability of the UHF-CCSD and UBD, and several UDFT methods for antiaromatic molecules. The diradical characters for parent antiaromatic molecules (**a**–**c**) are also calculated as shown in Table S8. The diradical character is 100% for **b** by the MkCCSD method in accord with all other computational methods examined here. On the other hand, the CASSCF and CASSCF-based MkCCSD computations predict the intermediate diradical character values for **a** and **c**.

4 Cyclobutadiene derivatives

4.1 Cyclobutadiene with polar substituents (d–f)

Bulky and polar substituents are often introduced into cyclobutadiene skeleton for the purpose of stabilization [102–104]. Menke et al. [98] and Eckert-Maksic et al. [99, 100] have already investigated cyano-substituted cyclobutadienes. They concluded that the CASPT2(X,X) (X = full π-active orbital space) was necessary for quantitative calculations of the S–T gaps of cyano-substituted cyclobutadienes. Here, variation of the S–T gap and diradical character is examined by introducing polar substituents: amino (**d**), formyl (**e**), and both amino and formyl (**f**) groups. Table 4 summarizes the total spin angular momentum for **d**–**f**. The spin densities on the carbon atoms of **d**–**f** for UHF solutions in both LS and HS states are summarized in the supporting Tables S9–S11. The behavior of $\langle S^2 \rangle$ values for both the LS and HS states are

Table 4 Total spin angular momentums $\langle S^2 \rangle$ of cyclobutadiene derivatives with polar substituents by the BS methods

Method	$C_4H_3(NH_2)$ (**d**)		$C_4H_3(CHO)$ (**e**)		$C_4H_3(NH_2)(CHO)$ (**f**)	
	LS	HS	LS	HS	LS	HS
UHF	1.2378	2.0176	1.4056	2.1588	1.3739	2.1353
UHF-MP2	1.1542	2.0023	1.2790	2.0974	1.2583	2.0834
UHF-CCSD	0.9952	2.0011	1.0236	2.0187	1.0375	2.0191
UBLYP	1.0264	2.0032	1.0280	2.0052	0.1182	2.0044
UB3LYP	1.0498	2.0044	1.0600	2.0115	0.1131	2.0106
UCAM-B3LYP	1.0694	2.0074	1.0874	2.0168	1.0773	2.0164
UBHandHLYP	1.0977	2.0049	1.1331	2.0324	1.1167	2.0303
ULC-BLYP	1.0965	2.0057	1.1214	2.0224	1.1130	2.0227
UBD	0.9798	2.0007	0.9854	2.0041	1.0039	2.0044

consistent with the results of the parent cyclobutadiene (**b**) with a few exceptions. The UBLYP and UB3LYP methods provide nearly closed-shell singlet solutions with $\langle S^2 \rangle^{LS} \sim 0.1$ for **f**. Table 5 summarize the S–T gap by the BS and MkCCSD methods. Table 5 shows that the $2J$ values for **d–f** are largely negative at the UHF level, while the results show the triplet ground state at the UHF-MP2 level. The UHF-CCSD and UHF-CCSD(T) methods predict the singlet ground state for **d–f**. The similar tendency is also obtained by UBD and UBD(T) as shown in Table 5. All

Table 5 The $2J$ values (kcal/mol) for **e–f** by the BS and MR methods

Method	$C_4H_3(NH_2)$ (**e**)	$C_4H_3(CHO)$ (**d**)	$C_4H_2(NH_2)(CHO)$ (**f**)
UHF	−53.0	−55.1	−39.4
UHF-MP2	15.2	7.8	18.1
UHF-CCSD	−8.2	−9.7	−4.8
UHF-CCSD(T)	−3.2	−4.5	−0.6
UBD	−7.3	−8.5	−4.0
UBD(T)	−3.6	−4.5	−0.9
UBLYP	−2.4	−3.3	−9.6
UB3LYP	−6.2	−7.2	−6.5
UCAM-B3LYP	−10.3	−11.3	−5.4
UBHandHLYP	−16.1	−17.1	−9.3
ULC-BLYP	−16.9	−18.1	−10.8
CASSCF(2,2)	0.5	3.4	−11.1
CASSCF(4,4)	−9.4	−9.6	−6.9
ROHF-MkCCSD (loc)[a]	−6.5	−7.1	−2.7
CASSCF-MkCCSD (loc)[a,b]	−7.3	−6.9	−4.5
UNO-MkCCSD (loc)	−7.3	−7.6	−4.3

[a] The localized active orbitals of ROHF MOs, CASSCF NOs, and UNOs are used

[b] The localized (2e,2o) active space based on the CASSCF(4e,4o) NOs are used

UDFT methods indicate the negative $2J$ values for **d–f**. The large magnitude of the $2J$ values for **f** calculated by UBLYP and UB3LYP are attributed to the nearly closed-shell singlet solutions. The $2J$ values by the UCAM-B3LYP are compatible with those of UHF-CCSD and UBD.

As in the case of **a** and **c**, the CASSCF(2,2) calculations for **d–f** give the delocalized solutions by substituting the electron-donating and electron-withdrawing group. The calculated Y values for **d–f** at the CASSCF(2,2) level do not exhibit complete diradical solutions as shown in Table S12. The inappropriate solutions for **d** and **e** cause the positive (triplet ground state) $2J$ values, while the nearly closed-shell singlet solution for **f** overestimates the stabilization of the singlet state as in the case of UBLYP and UB3LYP. On the other hand, the CASSCF(4,4) calculations including all 4π-orbitals give diradical solutions with $Y = 100\%$. The obtained $2J$ values represent the antiferromagnetic couplings. The S–T gap including the parent cyclobutadiene (**b**) decreases in the following order: **b** > **e** > **d** > **f** calculated by MkCCSD and most other methods. This indicates that the triplet state is more stabilized than the singlet state by the polar substituents. The complete diradical BS solutions are obtained outside of these exceptions, and the $2J$ value increases in the same order as **b**. The three types of localized active orbitals, which are compatible with those of **b**, are used for the MkCCSD computations. Note that the CASSCF(4,4) NOs are used instead of the poor CASSCF(2,2) NOs because the MkCCSD computations fail to converge with the use of localized CASSCF(2,2) NOs in contrast to **a** and **c**. The difference in $2J$ value is not remarkable for **d** and **e**, whereas the magnitude of the MkCCSD result with the use of the localized active orbitals of ROHF MOs is smaller than the other two by $\sim$2 kcal/mol. Judging from these MkCCSD results, the UBD with the AP method performs well for the π conjugated diradical systems [51, 105, 106].

4.2 Through-bond exchange coupling via cyclobutadiene (g, h)

Dougherty et al. [107] have already concluded that the ground state is a triplet for 1,3-dimethylenecyclobutadiene on experimental grounds. According to the spin vector model in Fig. 3e and f [8, 24], the 1,2- (**g**) and 1,3- (**h**) isomer of bis(methylene)cyclobutadiene are expected to show antireferromagnetic and ferromagnetic couplings, respectively. Table 6 summarizes the $\langle S^2 \rangle^{LS}$, $\langle S^2 \rangle^{HS}$ and $2J$ values for **g** and **h**. The Y values are summarized in Table 7. Figure 5 illustrates the populations of spin densities for these species. All methods employed here predict, respectively, the positive and negative $2J$ values for the **g** and **h**. Therefore computational results are consistent with

Table 6 The $\langle S^2 \rangle$ and 2*J* values (kcal/mol) for **g** and **h** by the BS and MR methods

Method	1,2-isomer (**g**)			1,3-isomer (**h**)		
	$\langle S^2 \rangle^{LS}$	$\langle S^2 \rangle^{HS}$	2 *J*	$\langle S^2 \rangle^{LS}$	$\langle S^2 \rangle^{HS}$	2 *J*
UHF	0.6848	2.2565	−78.4	0.9901	2.4451	44.1
UHF-MP2	0.5662	2.1671	−90.4	1.0092	2.3124	4.5
UHF-CCSD	0.1226	2.0290	−81.1	1.0847	2.0872	23.5
UHF-CCSD(T)	0.1266	2.0290	−82.7	1.0847	2.0872	15.0
UBD	0.0000	2.0083	−79.5	1.1030	2.0308	26.1
UBD(T)	0.0000	2.0083	−79.8	1.1030	2.0308	17.1
UBLYP	0.0000	2.0098	−75.3	0.9502	2.0240	13.3
UB3LYP	0.0000	2.0224	−74.9	0.9535	2.0568	19.6
UCAM-B3LYP	0.0000	2.0387	−74.5	0.9565	2.0981	23.6
UBHandHLYP	0.0000	2.0590	−71.3	0.9640	2.1414	28.6
ULC-BLYP	0.0000	2.0657	−73.6	0.9610	2.1559	28.6
CASSCF	0	2	−86.9	0	2	10.1
ROHF-MkCCSD	0	2	−82.7	0	2	20.0
CASSCF-MkCCSD	0	2	−84.2	0	2	19.5
UNO-MkCCSD	0	2	−83.4	0	2	19.8
ROHF-MkCCSD (loc)[a]	0	2	−84.1	0	2	19.3
CASSCF-MkCCSD (loc)[a]	0	2	−93.4	0	2	14.9
UNO-MkCCSD (loc)[a]	0	2	−83.7	0	2	16.6

[a] The localized active orbitals of ROHF MOs, CASSCF NOs, and UNOs are used

Table 7 The *Y* values (%) for **g** and **h** by the BS and MR methods

Method	1,2-isomer (**g**)	1,3-isomer (**h**)
UHF	2.7	67.8
UBD[a]	0.0	70.8
UBLYP	0.0	56.5
UB3LYP	0.0	57.3
UCAM-B3LYP	0.0	58.2
UBHandHLYP	0.0	60.5
ULC-BLYP	0.0	59.8
CASSCF	8.3	49.0
ROHF-MkCCSD	5.2	51.0
CASSCF-MkCCSD	5.1	51.0
UNO-MkCCSD	4.0	53.9

The corresponding effective bond order *B* (%) is give by 100-*Y*

Equation 6b is used

$Y = 2c_2^2$ is used

[a] The *Y* values are calculated in the Fermi vacuum

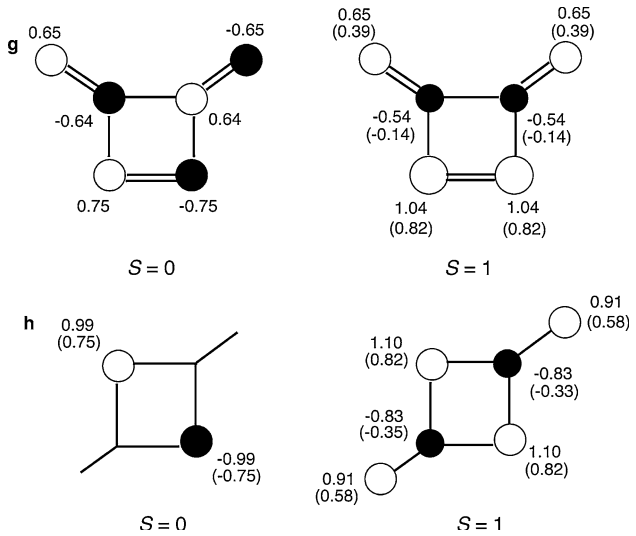

Fig. 5 Spin densities for **g** and **h** both in the singlet and triplet states calculated by UHF. Values in *parentheses* represent results calculated by UCAM-B3LYP

the prediction of the spin vector model in Figs. 3 and 5 qualitatively: namely singlet and triplet ground states, respectively, for **g** and **h**.

The $\langle S^2 \rangle^{LS}$ value for **g** obtained by UHF remains to be 0.685, indicating that the SP effect appears in the C = C bonds as shown in Fig. 5, while no spin density appears in the UDFT solutions for every exchange–correlation functional. The $\langle S^2 \rangle^{LS}$ values for **g** decrease with increasing the dynamical correlation corrections in the order of UHF > UHF-MP2 > UHF-CCSD. The spin contamination for **g** is not completely removed at the CCSD level, although the UHF-CCSD method greatly improves the UHF-MP2

solution. On the other hand, $\langle S^2 \rangle^{BS}$ value calculated by UBD is equal to zero. The $2J$ values range from −78.4 to −79.8 kcal/mol for UHF, UBD and UBD(T), and from −71.3 to −75.3 kcal/mol for the UDFT methods. For the MkCCSD results, the S–T gaps (2 J) with the use of both delocalized and localized natural orbitals are ∼ −84 kcal/mol except for MkCCSD starting from the localized active orbitals of CASSCF NOs (−93 kcal/mol). The MkCCSD calculation does not depend on the reference orbital since the electronic structure of **g** is nearly closed-shell singlet.

Since the radical sites exist in **h**, large spin densities appear on C3 and C5 atoms in the LS solutions even at the UDFT levels, in contrast to **g**, as shown in Tables S13 and S14. According to the natural orbital analysis, the Y value ranges from 49.0 to 70.8% as shown in Table 7. The relatively large overlap between the C3 and C5 sites decreases the Y value. The $\langle S^2 \rangle^{HS}$ value obtained by UHF (2.445) is larger than 2.0, indicating the strong SP effect as shown in Fig. 5. Therefore, it provides the positive large $2J$ value. The inclusion of the dynamical correlation corrections by UHF-CCSD and UBD suppress the excess of the SP effects. As for UDFT methods, the spin populations on each carbon atom correlate with HF exchange, and the magnitude of $2J$ value increases as UBLYP < UB3LYP < UBHandHLYP. The range-separated ULC-BLYP provides the $2J$ value same as that of UBHandHLYP, while the UCAM-B3LYP result lies between UB3LYP and UBHandHLYP. The S–T gaps obtained by the MkCCSD computations do not depend on the reference orbitals when the delocalized ones are used. On the other hand, the calculated $2J$ values vary with the localized reference orbitals, ranging between 14.9 and 19.3 kcal/mol. The $2J$ values are 15.0 and 17.1 kcal/mol, respectively, by UHF-CCSD(T) and UBD(T). Therefore these methods reproduce the MkCCSD results based on the localized natural orbitals.

5 Discussions and concluding remarks

5.1 Chemical indices

In this paper we have calculated effective bond order and diradical character values to elucidate the nature of chemical bonds of parent antiaromatic molecules and their derivatives. The effective bond order values are defined for both the spin-projected BS and MR solutions as shown in Tables S5–S7. These indices are useful for extraction of common chemical pictures from the BS and MR calculations. However, we do not discuss the unpaired electron density and spin correlation functions. The unpaired electron density is defined by the square of spin density and it is directly related to the Coulomb hole between electrons with opposite spins [108, 109]. Therefore the magnitude of the spin density appeared in the BS solutions is nothing but the size of the Coulomb hole from the electron correlation theory [24]. On the other hand, the product of the spin densities on each site just corresponds to the classical part of the spin correlations function defined by the second-order density matrix [108, 109]. This means that the sign of the spin densities is directly related to the sign of spin correlation functions: negative spin density product corresponds to the antiferromagnetic spin correlations and positive spin density product corresponds to ferromagnetic spin correlations. The spin vector model in Fig. 3 represents these spin correlations with classical vectors. The physical background and mathematical expressions for these chemical indices are given in Refs. [24, 110].

5.2 Through-bond exchange coupling

Imamura and Hoffmann have presented seminal papers concerning with through-bond and through-space interactions [111, 112] in late 1960s. Imamura and Aoki and their collaborators [113, 114] have further developed the elongation methods for elucidation and computations of electronic and spin structures of extended systems such as polymers. We have applied the UHF method to elucidate through-bond exchange couplings between radical groups introduced into π-networks [115]. For example, ferromagnetic and antiferromagnetic polymers are easily designed on the basis of the spin vectors models in Fig. 3 assisted with the spin correlation functions obtained by the BS calculations as illustrated in Fig. 6 [24].

Mitani et al. [66–69] have performed extensive hybrid UDFT calculations of the diradical and polyradical systems to elucidate the through-bond effective exchange integrals in diradicals and polyradicals. Very recently, we made a comparison of the $2J$ value for through-bond exchange interactions in oxyallyl between several BS and MR methods [116]. It was concluded that an appropriate description of nondynamical and dynamical correlation is essential even for such small species. Therefore benchmark

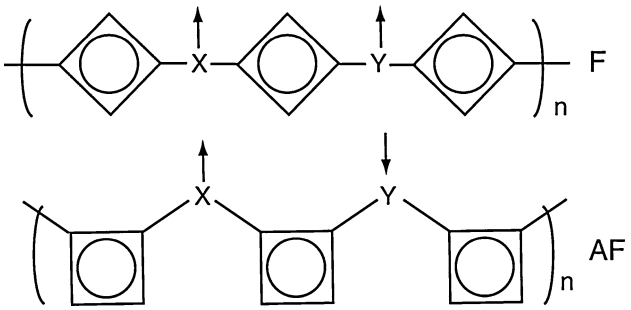

Fig. 6 Magnetic polymers with ferromagnetic (F) and antiferromagnetic (AF) spin alignments constructed of cyclobutadiene skeletons. *X* denotes the radical site with local spins such as –CR–, –NO–

tests of small diradical systems by conducting the accurate MkCCSD computations are useful for the elucidation of scope and applicability of various BS calculations.

5.3 Concluding remarks

In this paper, we have performed systematic comparisons of MkCCSD and BS methods concerning with singlet–triplet energy gaps (2 *J*) and diradical characters of typical diradical species: antiaromatic molecules (**a**–**c**), cyclobutadiene derivatives with polar substituents (**d**–**f**), cyclobutadiene with radical substituents (**g**–**h**). From these comparisons, we have pointed out that (i) spin-contamination of the UHF (or spin-unrestricted Brueckner) determinant-based CC solutions is non-negligible and it arises mainly from triplet state; (ii) the AP method is also applicable to the inclusion of the perturbative triple corrections (T) such as UHF-CCSD(T); (iii) NOs of BS solutions are sufficient as reference orbitals of MkCCSD calculations; (iv) RHF-CCSD often fails in calculation of diradical species with strong diradical characters; (v) chemical indices are useful for elucidation of the nature of chemical bonds of diradical species. We employed four types of orbitals for MkCCSD, i.e. ROHF MOs, CASSCF NOs, UNOs and DNOs. The dependence of the singlet–triplet gaps on these NOs is small in the case of diradicals examined here. This in turn indicates that NOs obtained from BS computations such as hybrid UDFT are directly utilized for the reference orbitals for successive MkCCSD computations of quasi-degenerate electronic systems. Furthermore, size-consistent correction is feasible for MkCCSD with the use of localized active orbitals. The UDFT methods are modified to reproduce qualitatively good results that are compatible with highly accurate ab initio methods in spite of their low computational costs; the magnetic effective DFT method is such an example [117]. The $\langle S^2 \rangle$ values predicted by the non-interaction procedure are comparable to the XLSD and XGGA schemes. The MkCCSD computations of parent diradicals with the use of BS NOs as reference orbitals provide useful and reliable 2*J* values for calibration and construction of effective hybrid UDFT functionals for related large diradical systems. This study also shows that the highly correlated BS methods with the AP correction as well as MkCCSD have potential to provide reference data for the design of a new exchange–correlation functional that is suitable for diradical molecules. Thus, further developments of both symmetry-adapted MR methods and BS methods should be imperative for describing the electronic structures of complicated polyradical systems, followed by the design of molecular-based magnetic materials.

Acknowledgments This work has been supported by Grants-in-Aid for Scientific Research (KAKENHI) (Nos. 21550014, 19750046, 19350070) from Japan Society for the Promotion of Science (JSPS) and that on Grant-in-Aid for Scientific Research on Innovative Areas ("Coordination Programming" area 2170, No. 22108515) from the Ministry of Education, Culture, Sports, Science and Technology (MEXT). T. S. is grateful for the Research Fellowships from JSPS for Young Scientists.

Appendix

The acronyms given in the text are summarized in Table S15 in the Supporting Information.

References

1. Salem L (1982) Electrons in chemical reactions: first principles. Wiley, New York
2. Borden WT (1982) Diradicals. Wiley, New York
3. Kahn O (1993) Molecular magnetism. VCH Pub, New York
4. Nagakura S (1998) Functionality of molecular systems 1. From Molecules to Molecular Systems, Springer, Tokyo
5. Itoh K, Kinoshita M (2000) Molecular magnetism: new magnetic materials. Gordon & Breach Pub, New York
6. Nakamura A, Ueyama N, Yamaguchi K (2002) Organometallic conjugation. Kodansha, Springer, Tokyo
7. McConnell HH (1963) J Chem Phys 39:1910
8. Yamaguchi K (1975) Chem Phys Lett 35:230
9. Kollmar H, Staemmler V (1978) Theor Chim Acta 48:223
10. Miller JS, Epstein AJ (1994) Angew Chem Int Ed 33:385
11. Ginsburg AP (1980) J Am Chem Soc 102:111
12. Noodleman L, Davidson ER (1986) Chem Phys 109:131
13. Yamaguchi K, Fukui H, Fueno T (1986) Chem Lett 625
14. Ruiz E, Cano J, Alvarez S, Alemany P (1999) J Comput Chem 20:1391
15. Löwdin P-O (1955) Phys Rev 97:1474
16. Nesbet RK (1958) Phys Rev 109:1632
17. Löwdin P-O (1959) Adv Chem Phys 2:207
18. Takatsuka K, Nagase S, Yamaguchi K, Fueno T (1977) J Chem Phys 67:2527
19. Bartlett RJ (1981) Ann Rev Phys 32:359
20. Chen W, Schlegel HB (1994) J Chem Phys 101:5957
21. Stanton JF (1994) J Chem Phys 101:371
22. Yuan H, Cremer D (2000) Chem Phys Lett 324:389
23. Yamaguchi K (1980) Int J Quant Chem S14:269 doi: 10.1002/qua.560180831
24. Yamaguchi K (1990) In Self-consistent field, Theory and applications (Carbo R, Klobukowski M (Eds)). Elsevier, Amsterdam p 727
25. Bartlett RJ (2002) Int J Mol Sci 3:579
26. Yamaguchi K (1983) J Mol Struct (THEOCHEM) 103:101
27. Yamaguchi K, Yamanaka S, Nishino M, Takano Y, Kitagawa Y, Nagao H, Yoshioka Y (1999) Theor Chem Acc 102:328
28. Kawakami T, Takeda R, Nishihara S, Saito T, Shoji M, Yamada S, Yamanaka S, Kitagawa Y, Okumura M, Yamaguchi K (2009) J Phys Chem A 113:15281
29. Jeziorski B, Monkhorst HJ (1981) Phys Rev A 24:1668
30. Mukherjee D, Pal S (1989) Adv Quant Chem 20:292
31. Mahapatra US, Datta B, Mukherjee D (1999) J Chem Phys 110:6171
32. Paldus J, Li X (1999) Adv Chem Phys 110:1
33. Evangelista FA, Allen WD, Schaefer HF III (2006) J Chem Phys 125:154113

34. Evangelista FA, Allen WD, Schaefer HF III (2007) J Chem Phys 127:024102
35. Evangelista FA, Prochnow E, Gauss J, Schaefer HF III (2010) J Chem Phys 132:074107
36. Miralles J, Castell O, Caballol R, Malrieu JP (1993) Chem Phys 172:33
37. Andersson C, Malmqvist PA, Roos BO (1992) J Chem Phys 96:1218
38. Angeli C, Cimiraglia R, Evangelisti S, Leininger T, Malrieu JP (2001) J Chem Phys 114:10252
39. Queralt N, Tratiel D, de Graaf C, Caballol R, Cimiraglia R, Angeli C (2008) J Comput Chem 29:994
40. Chan GKL, Sharma S (2011) Annu Rev Phys Chem 62:465. doi: 10.1146/annurev-physchem-032210-103338
41. Takeda R, Yamanaka S, Yamaguchi K (2002) Chem Phys Lett 366:321
42. Yamanaka S, Nakata K, Takada T, Kusakabe K, Ugalde JM, Yamaguchi K (2006) Chem Lett 35:242
43. Miehlich B, Stoll H, Savin A (1997) Mol Phys 91:527. doi: 10.1080/002689797171418
44. Malcolm NO, McDouall JJ (1998) Chem Phys Lett 282:121
45. Gräfenstein J, Cremer D (2000) Chem Phys Lett 316:569
46. Gräfenstein J, Cremer D (2005) Mol Phys 103:279
47. Gusarov S, Malmqvist P-Å, Lindh R, Roos BO (2004) Theor Chem Acc 112:84
48. Weimer M, Sala FD, Görling A (2008) J Chem Phys 128: 144109
49. Bartlett RJ (2009) Chem Phys Lett 484:1
50. Yamanaka S, Nishihara S, Nakata K, Yonezawa Y, Kitagawa Y, Kawakami T, Okumura M, Takada T, Nakamura H, Yamaguchi K (2010) In Recent Progress in Coupled Cluster Methods: Theory and Applications, (Paldus J (Ed)), Springer, New York
51. Nishihara S, Yamanaka S, Saito T, Kitagawa Y, Kawakami T, Okumura M, Yamaguchi K (2010) Int J Quant Chem 110:3015
52. Handy NC, Pople JA, Head-Gordon M, Raghavachari K, Trucks GW (1989) Chem Phys Lett 164:185
53. Kobayashi R, Amos RD, Handy NC (1991) Chem Phys Lett 184:195
54. Purvis GD III, Sekino H, Bartlett RJ (1988) Collect Czech Chem Commun 53:2203
55. Wang J, Becke AD, Simith VH Jr (1995) J Chem Phys 102:3477
56. Cohen AJ, Tozer DJ, Handy NC (2007) J Chem Phys 126:214104
57. Yamaguchi K (1979) Chem Phys Lett 66:395
58. Yamaguchi K (1979) Chem Phys Lett 68:477
59. Paldus J, Cizek J (1967) J Chem Phys 47:3976
60. Fukutome H (1968) Prog Theoret Phys 40:998
61. Pople JA, Nesbet RK (1954) J Chem Phys 22:571
62. Amos AT, Hall GG (1961) Proc R Soc Lond A 263:483
63. Yamaguchi K (1975) Chem Phys Lett 33:330
64. Yamaguchi K (1980) Int J Quant Chem 18:101
65. Yamaguchi K, Yabushita S, Fueno T, Kato S, Morokuma K, Iwata S (1980) Chem Phys Lett 71:563
66. Mitani M, Takano Y, Yoshioka Y, Yamaguchi K (1999) J Chem Phys 111:1309
67. Mitani M, Yamaki D, Yoshioka Y, Yamaguchi K (1999) J Chem Phys 111:2283
68. Mitani M, Mori H, Takano Y, Yamaki D, Yoshioka Y, Yamaguchi K (2000) J Chem Phys 111:2283
69. Mitani M, Yamaki D, Takano Y, Kitagawa Y, Yoshioka Y, Yamaguchi K (2000) J Chem Phys 113:10486
70. Noodleman L, Lovell T, Han WG, Li J, Himo F (2004) Chem Rev 104:459
71. Siegbahn PEM, Borowski T (2006) Acc Chem Res 39:729
72. Neese F (2006) J Biol Inorg Chem 11:702
73. Neese F (2009) Coord Chem Rev 253:526
74. Bencini A (2008) Inorg Chim Acta 361:3820
75. Gherman BF, Cramer CJ (2009) Coord Chem Rev 253:723
76. Becke AD (1988) Phys Rev A 38:3098
77. Frisch MJ, Trucks GW, Schlegel HB, Scuseria GE, Robb MA, Cheeseman JR, Scalmani G, Barone V, Mennucci B, Petersson GA, Nakatsuji H, Caricato M, Li X, Hratchian HP, Izmaylov AF, Bloino J, Zheng G, Sonnenberg JL, Hada M, Ehara M, Toyota K, Fukuda R, Hasegawa J, Ishida M, Nakajima T, Honda Y, Kitao O, Nakai H, Vreven T, Montgomery JA Jr, Peralta JE, Ogliaro F, Bearpark M, Heyd JJ, Brothers E, Kudin KN, Staroverov VN, Kobayashi R, Normand J Raghavachari K, Rendell A, Burant JC, Iyengar SS, Tomasi J, Cossi M, Rega N, Millam NJ, Klene M, Knox JE, Cross JB, Bakken V, Adamo C, Jaramillo J, Gomperts R, Stratmann RE, Yazyev O, Austin AJ, Cammi R, Pomelli C, Ochterski JW, Martin RL, Morokuma K, Zakrzewski VG, Voth GA, Salvador P, Dannenberg JJ, Dapprich S, Daniels AD, Farkas Ö, Foresman JB, Ortiz JV, Cioslowski J, Fox DJ (2009) Gaussian 09, Revision A.2, Gaussian, Inc., Wallingford CT
78. Schmidt MW, Baldridge KK, Boatz JA, Elbert ST, Gordon MS, Jensen JH, Koseki S, Matsunaga N, Nguyen KA, Su SJ, Windus TL, Dupuis M, Montgomery JA (1993) J Comput Chem 14:1347
79. Gordon MS, Schmidt MW (2005) In: Theory and Applications of Computational Chemistry: the first forty years (Dykstra CE, Frenking G, Kim KS, Scuseria, GE (Eds)). Elsevier, Amsterdam p 1167
80. Crawford TD, Sherrill CD, Valeev EF, Fermann JT, King RA, Leininger ML, Brown ST, Janssen CL, Sedil ET, Kenny JP, Allen WD (2007) J Comput Chem 28:1610
81. Dunning TH Jr (1989) J Chem Phys 90:1007
82. Kendall RA, Dunning TH Jr, Harrison RJ (1992) J Chem Phys 96:6796
83. Lee C, Yang W, Parr RG (1988) Phys Rev B 37:785
84. Becke AD (1993) J Chem Phys 98:5648
85. Iikura H, Tsuneda T, Yanai T, Hirao K (2001) J Chem Phys 115:3540
86. Yanai T, Tew D, Handy NC (2004) Chem Phys Lett 393:51
87. Breslow R (1968) Angew Chem Int Ed 7:565
88. Buenker RJ, Peyerimhoff SD (1968) J Chem Phys 48:354
89. Borden WT (1975) J Am Chem Soc 97:5968
90. Yamaguchi K, Nishio A, Fueno T (1977) Chem Lett 971
91. Kollmar H, Staemmler V (1977) J Am Chem Soc 99:3583
92. Borden WT, Davidson ER (1981) Acc Chem Res 14:69
93. Voter AF, Goddard WA III (1986) J Am Chem Soc 108:2830
94. Merrill GN, Kass SR (1997) J Am Chem Soc 119:12322
95. Filatov M, Shaik S (1999) J Chem Phys 110:116
96. Levchenko SV, Krylov AI (2004) J Chem Phys 120:175
97. Karadakov PB (2008) J Phys Chem A 112:7303
98. Menke JL, Patterson EV, McMahon RJ (2010) J Phys Chem A 114:6431
99. Eckert-Maksic M, Vazdar M, Barbatti M, Lischka H, Maksic ZB (2006) J Chem Phys 125:064310
100. Eckert-Maksic M, Lischka H, Maksic ZB, Vazdar M (2009) J Phys Chem A 113:8351
101. Wasserman E, Hutton RS (1977) Acc Chem Res 10:27
102. Balley T, Masamune S (1980) Tetrahedron 36:343
103. Balley T (2006) Angew Chem Int Ed 45:6616
104. Matsuo T, Sekiguchi A (2004) Bull Chem Soc Jpn 77:211
105. Saito T, Nishihara S, Yamanaka S, Kitagawa Y, Kawakami T, Okumura M, Yamaguchi K (2010) Mol Phys 108:2533
106. Nishihara S, Saito T, Yamanaka S, Kitagawa Y, Kawakami T, Okumura M, Yamaguchi K (2010) Mol Phys 108:2559
107. Snyden GT, Dougherty DA (1989) J Am Chem Soc 111:3927
108. Yamaguchi K, Fueno T (1977) Chem Phys 19:171
109. Yamaguchi K (1978) Chem Phys 29:117

110. Yamaguchi K, Yamanaka S, Isobe H, Kawakami T, Kitagawa Y, Takeda R, Saito T, Nishihara S, Okumura M (2009) AIP Conf Proc 1108:20
111. Imamura A, Hoffmann R (1968) J Am Chem Soc 90:5379
112. Hoffmann R, Imamura A, Hehre WJ (1968) J Am Chem Soc 90:1499
113. Imamura AY, Maekawa K (1991) J Chem Phys 95:5419
114. Orimoto Y, Gu FL, Korchowiec J, Imamura A, Aoki Y (2010) Theoret Chem Acc 125:493
115. Yamaguchi K, Toyoda Y, Fueno T (1987) Syntetic Metals 19:81
116. Saito T, Nihishara S, Yamanaka S, Kitagawa Y, Kawakami T, Yamada S, Isobe H, Okumura M, Yamaguchi K (2011) Theor Chem Acc doi:10.1007/s00214-011-0914-z
117. Nakanishi Y, Kitagawa Y, Saito T, Kataoka Y, Matsui T, Kawakami T, Okumura M, Yamaguchi K (2009) Int J Quant Chem 109:3632